# EDGE/REGION-BASED SEGMENTATION AND RECONSTRUCTION OF UNDERWATER ACOUSTIC IMAGES BY MARKOV RANDOM FIELDS

Vittorio Murino

DIMI - Dept. of Mathematics & Computer Science
University of Udine, Via delle Scienze 208
33100 Udine, Italy – Email: swan@dimi.uniud.it

Andrea Trucco

DIBE - Dept. of Biophysical & Electronic Engineering
University of Genova, Via all'Opera Pia 11A
16145 Genova, Italy - Email: fragola@dibe.unige.it

***Abstract*** – This paper describes a technique for the reconstruction and segmentation of three-dimensional acoustical images using a coupled Random Fields able to actively integrate confidence information associated with acquired data. Beamforming, a method widely applied in acoustic imaging, is used to build a three-dimensional image, associated point by point with another kind of information representing the reliability (i.e., "confidence") of such an image. Unfortunately, this kind of images is plagued by several problems due to the nature of the signal and to the related sensing system, thus heavily affecting data quality. Specifically, speckle noise and the broad directivity characteristic of the sensor lead to very degraded images. In the proposed algorithm, range and confidence images are modelled as Markov Random Fields whose associated probability distributions are specified by a single energy functional. A three-fold process has been applied able to reconstruct, segment, and restore the involved acoustic images exploiting both types of data. Our approach showed better performances with respect to other MRF-based methods as well as classical methods disregarding reliability information. Optimal (in the Maximum A-Posteriori probability sense) estimates of the 3D and confidence images are obtained by minimizing the energy functional by using simulated annealing.

## 1. INTRODUCTION

Image reconstruction, restoration, and segmentation are classical low-level processes useful for any subsequent higher-level vision task such as object recognition and image interpretation [1,2]. Unfortunately, sensed data are always degraded by the transfer function of the acquiring device, so that adequate processing is required to recover actual world information embedded in cluttered data.

These problems are enforced in the case of acoustical sensor systems treated in this work. Actually, although acoustical systems can implicitly recover three-dimensional (3D) information, the inherent nature of the acoustic signals causes the generation of very noisy and cluttered images, difficult to process for high-level tasks. Therefore, it is absolutely necessary to use efficient techniques to reconstruct and segment acoustic images in order to recover the real three-dimensional structure of the observed scene.

This paper aims at showing how reconstruction of acoustic 3D images can be improved by integrating two types of information provided by an acoustical system, an actual range image and a "confidence" image associated point by point with each depth measure denoting its reliability. Unfortunately, the acoustical image formation process (i.e., beamforming [3,4]) exhibits two critical problems, speckle noise due to the coherence of the acoustical signal [5,6], and side lobes due to the non-ideal sensor characteristics (beam power pattern) [3].

Typically, acoustic data are on-line visualized in real sonar systems by simply thresholding the acquired rough signals, i.e., by considering only sampled signal values above a certain threshold [4]. Although this method is very fast, it produces results of poor quality, as compared with more robust and *ad-hoc* methods. The MRF approach [7,10,11] is one of these methods that was specifically used for range image segmentation. In [12], range and intensity (optical) images were separately segmented by fusing boundary information at multiple scales by using a nonlinear MRF algorithm. The proposed energy functional embedded classical smoothness and observation closeness constraints, a line process and a coupling term between adjacent scales. In [13], an MRF model-based segmentation scheme was proposed that was able to discriminate between jump and crease edges by using the related likelihood ratios, computed on the basis of local statistical operators, and by embedding them into an MRF framework. In [14], the "gradient limit effects" [11] were reduced by fusing registered range and intensity images by an extended weak membrane model enforcing the line process. The fusion occurred by means of a coupled term in the energy function that penalized different edge configurations in the two kinds of images. A similar method for the fusion of range and intensity images was followed in [15] by integrating in a single framework edge detection, semantic labelling and surface reconstruction.

Other works deal with the reconstruction and segmentation of range images (see also [8,9]), but none of these addresses the more complex problems related to 3D acoustic imaging, nor the coupled segmentation and reconstruction issues using actively confidence information.

Considering specific literature on acoustical images, in [16], a segmentation algorithm based on surface fitting was used to recover 3D structures from sparse data derived by simulated 3D sonar images. Restoration of side scan sonar images by using Simulated Annealing and Iterative Conditional Modes was addressed in [17]. Here, restoration was intended as the process of reducing the speckle noise modelled as having a Rayleigh or Gaussian probability density function. Error evaluation in the context of the reconstruction of sea bed bathymetric data was addressed in [18] by using the Graduated Non-Convexity [11] minimization method. Here, to reconstruct correct bathymetric data acquired with a multibeam sonar, either a weak membrane or a thin-plate model [2] was used, and a line process was included to remove the smoothness constraint at surface boundaries. Segmentation of images acquired by a multibeam echosounder by MRFs is also addressed in [19]. By arranging the acoustical map on the basis of the acquisition parameters, they devise a classical MRF process modeling the prior energy as weighting coefficients depending on its geometrical location and the observation energy term as a $\chi^2$ distribution.

The problem of reconstruction of acoustic data extracted by an acoustical multibeam system was already addressed by the authors in [20,21]. It should be noticed that these works were the first attempts to processing such kind of data, i.e., representing explicitly 3D and related confidence measures. The strength of these methods was the joint use of both information in the definition of a single energy function to be minimized, unlike other methods which use a reliability (variance) measure in a passive way to estimate the goodness of the results [2]. In [20], it is proposed an energy functional jointly considering the dual information in such a way that, only those pixels belonging to the 3D image showing high confidence are retained, whereas the 3D values were assumed unreliable in those pixels showing low confidence. In [21], this mechanism is evolved in the definition of a different functional which takes into account the physical significance of the coupling term between 3D and confidence images.

In the present work, we further investigate the reconstruction and restoration processes performed by MRFs enhancing the process by devising an energy functional able to detect edge points by exploiting both range and confidence information. The whole estimation process is inherently three-fold, i.e., reconstruction, restoration, and segmentation are performed simultaneously, taking mutually into account all types of information available. Consequently, the reconstruction process evolves considering the segmentation of the images in edges (line field) and regions (confidence field). In general, the estimated confidence values are utilized to perform smoothness inside object surfaces preventing smoothing at boundaries between object and background as well as among different objects.

The presented results are also compared with classical MRF-based and deterministic methods for reconstruction showing better performances obtained by using confidence in an active way. It should be also noted here that, although the visual quality of the estimated images might seem poor, they represent very good results as compared with those obtained by other methods for the same kind of images. In fact, the quality of acoustic images is very poor with respect to the quality of images acquired by a laser range finder for instance.

The paper is organized as follows. In Section 2, the MRF approach is presented, with special emphasis on the energy functional formulation. In Section 3, results are presented and discussed and, finally, conclusions are drawn in Section 4.

## 2. THE EDGE/REGION BASED MRF METHOD

In short, an MRF can be defined on a lattice field of random variables in which the probability of a specific realization is given by a Gibbs distribution (Hammersley-Clifford theorem [7]). The energy function associated with such distribution can be computed by summing only *local* contributions with respect to a neighbourhood system defined on the lattice. Therefore, the energy minimization leads to the best estimate. For a complete formal definition of an MRF the reader can refer to [7].

Let us consider $Y = (Y_S, Y_Z)$ (i.e., the observable random field pair) as input data, where $Y_S$ is related to the M×M confidence image S and $Y_Z$ is related to the M×M range image Z to be estimated, respectively. In addition, a line field L is also considered representing the edge map to be estimated. We regard Z, S, and L as sample realizations of an MRF for a given neighbourhood system; then, the process of coupled segmentation and reconstruction lies in estimating the true fields Z, S, and L, given the noisy input image pair Y. Therefore, we formulate the reconstruction, restoration, and segmentation problems in terms of maximization of the a-posteriori probability associated with the prior and sensor models by devising a unique joint energy functional.

As prior models, a weak membrane energy term is assumed for reconstruction (as previously proposed in [7,10,11]) and, for restoration, a function based on the physical acquisition process has been devised, enforcing those points associated to an object and penalizing the others. As sensor models, a Gaussian modelling is used for restoration, whereas, for reconstruction, the usual data compatibility term is utilized [2,7,22]. Moreover, we include in the global energy function a modulating term weighting the sensor model of the field Z. These functions, expressed in terms of S, take into account the physical significance of the map Z which is built by detecting the maximum peak for each beam signal. In this

way, since the restoration of the field S is performed together with the reconstruction of Z, the latter process is actively driven taking strongly into account how data are acquired. In other words, this formulation allows us to integrate confidence information to bias the contributions of the prior and sensor models of Z in order to get a more accurate final estimation. Finally, considering the field L, clique potentials have been included to favour certain edge configuration, simultaneously allowing to bias the smoothness constraint favouring it only in those regions where no edge points are present.

Therefore, under the assumption of additive i.i.d. (independent, identically-distributed) Gaussian noise affecting the images and using the Hammerslay-Clifford equivalence and the Bayes criterion, we can write the a-posteriori joint energy function (related to the a-posteriori probability [7]) as the sum of several terms:

$$E(Z,S,L/Y_Z,Y_S)=E_p(Z,S,L)+E_{obs}(Y_Z,Y_S/Z,S,L)= \\ E_p(Z/S,L)+E_p(L/S)+E_p(S)+E_{obs}(Y_Z/Z,S,L)+E_{obs}(Y_S/Z,S,L) \quad (1)$$

where $E_p$ are functions related to a-priori modelling and $E_{obs}$ are functions related to observation models. Thus, Eq. (1) represents the global energy function composed of the a-priori and observation models of the fields (Z,S,L). Due to the specific process involved, the models can be subdivided into energy terms as a function of only one field influenced by others. The a-priori energy term of Z (weak membrane [2,7]) is modulated by a function of the line field L:

$$E_p(Z/S,L)=\sum_{i\in Z}\sum_{j\in N_i}E_p(z_i,z_j)\cdot(1-l_{ij})=\sum_{i\in Z}\sum_{j\in N_i}(z_i-z_j)^2\cdot(1-l_{ij}) \quad (2)$$

where i is a generic pixel site, $z_i$ is the value of the pixel i of the range field Z, and $N_i$ is the neighbourhood of the pixel i (on both fields Z, S and L), and $l_{ij}$ is a term which is 1 when an edge point is present between the pixel *i* and its neighbour *j*, and zero otherwise. Actually, this term depends by S through the estimated line field L. This makes it possible to apply the smoothness constraint only in homogeneous regions. We consider the same first-order neighbourhood system on all of the fields.

Correspondingly, the coupled observation model in Eq. (1) has been divided into two separate terms, given the conditional independence of the $Y_z$ and $Y_s$ fields given (Z,S). Therefore, the term $E_{obs}(Y_z/Z,S,L)$ is not affected by L, and can be written as (AGN modelling):

$$E_{obs}(Y_Z/Z,S)=\sum_{i\in Z}E_{obs}(y_{z_i}/z_i)V_b(s_i)=\frac{1}{2\sigma_z^2}\sum_{i\in Z}(z_i-y_{z_i})^2V_b(s_i) \quad (3)$$

where $y_{z_i}$ is the value of the pixel i of the observation $Y_z$, $s_i$ is the value of the pixel i of the confidence field S, and $V_b(s_i) = \sqrt{s_i}, \forall i \in S$ is a modulating function that reinforces or weakens the observation contribution of Z. Practically, the observed image can be more or less reliable and, on this basis, the prior model of Z can be more or less emphasized. This function reaches the maximum value, equal to 1, if the confidence of the pixel $z_i$ is 1, stressing the data compatibility constraint. The square root operation is used to weight, in a different manner, low- and high-confidence points enhancing the observation constraint also for pixels having weak confidence levels.

Concerning the restoration of the field S, it should be noted that the Z and L estimates would not have to affect the prior and sensor models of confidence, then $E_{obs}(Y_S/Z,S,L) = E_{obs}(Y_S/S)$. In fact, the map S represents a true confidence associated pixel by pixel with the map Z, in that low S values do not imply an incorrect Z value but only less reliability in the correctness of that value. As a consequence, the prior knowledge on the field S should force the observed confidence map to become binary, i.e., 1 (maximum confidence) where an object is present, and 0 otherwise. The function related to the prior model is:

$$E_p(S)=\sum_{i\in S}E_p(s_i)=\sum_{i\in S}\left(s_i-s_{i,t}\right)^2 \quad (4)$$

where the value $s_{i,t}$ can be 0 or 1 on the basis of the number of neighbourhood pixels whose value is larger than a fixed threshold $T_c$. This threshold is set considering the beam pattern profile, i.e., more precisely, the side lobe level. On the basis of this level, it is possible to calculate the attenuation of the beam signals due to the side lobes, likely allowing to separate confident from non-confident pixels. In practice, the term $s_{i,t}$ is equal to 1 if most of the pixels in the neighbourhood (of the first order) of $s_i$ are above the threshold $T_c$, and is equal to 0 otherwise.

For the sensor model of S, a Gaussian model is adopted:

$$E_{obs}(Y_s/S)=\sum_{i\in S}E_{obs}(y_{s_i}/s_i)=\frac{1}{2\sigma_s^2}\sum_{i\in S}(s_i-y_{s_i})^2 \quad (5)$$

where $y_{s_i}$ is the value of the pixel i of observation $Y_S$.

The energy terms related to the line process should take into account the different typologies of edge points, i.e., those related to the confidence image (discriminating between objects and background) and to the range image (when objects at different distances are present). Therefore, the energy contributions due to the line field are divided in 2 terms :

$$E_p(L/S)=\beta\sum_{i\in L}\sum_{c\in C_l}V_c+\gamma\sum_{i\in L}\sum_{j\in N_i}\left[r_i(N_i)-l_{ij}\right]^2 \quad (6)$$

The first term of the RHS depends on a-priori knowledge about certain edge configurations. Specifically, $V_C$ are the potentials associated to the possible cliques $c\in C_l$ (i.e., a subsets of sites that are neighbor each other) aimed at penalizing certain edge configurations, and $\beta$ is a constant factor. The last term

takes into account the two possible types of edge, i.e., those derived by the confidence image and by the range one. The factor $l_{ij}$ is defined as before, $r_i(\cdot)$ is a binary term depending on the neighbouring system of the field S. This term is equal to 0 if the majority of the pixel $s_i$ is below or larger than the threshold $T_C$ (set by analyzing the side lobe level of the sensor used, like before), and 1 otherwise, and $\gamma$ is a constant factor. This means that, inside homogeneous S areas (i.e., mostly confident or mostly non confident), edge points are discouraged, whereas are favoured in uncertain S areas as well as between objects at different distances.

The minimization of the global energy function leads to the optimal (in the MAP sense) reconstructed and restored estimates. To this end, we adopted a simulated annealing procedure in which the fields Z, S, and L evolve iteratively in a set of sample configurations in order to achieve the optimal ones. The fields are alternately changed according to a process similar to the dual process of restoration and edge-extraction described in [10].

## 3. RESULTS AND DISCUSSION

The proposed algorithm was tested on both real and simulated acoustic 3D images. In the latest case, a simulator of active imaging systems whose output signals were processed by a beamformer was used. Generally, the acoustic scattering from a surface can be simulated by adding the effects produced by many punctiform ideal scatterers placed on the surface [23]. After the distribution of the points and the scene insonification, the signal received by a given array sensor was computed on the basis of the sum of the spherical waves emitted from the scatterers composing the objects. This kind of simulation is widely accepted as the correct mode of generation of acoustic images, as it makes it possible to generate very realistic images of slightly rough objects affected by speckle noise.

The synthetic example consists of a single but quite complicated object for an acoustic imaging process: it is an inclined rhomb with a circular inside hole, namely, a "rhomb" scene. The distance of the rhomb from the array ranges from 4.5 m to 4.7 m. The principal diagonal of the rhomb is 1.1 m long. Inside the rhomb, a circular hole with a radius of 0.2 m is present, increasing the difficulty of the segmentation and reconstruction operations. Starting from the noisy images in Figs. 1(a) and 1(b) for range and confidence data, respectively, the proposed algorithm aims at obtaining image representations as equal as possible to the ideal images, represented by a rhomb of a different color over a white background. In the ideal range image, the rhomb is characterized by a grey-level profile linearly variable with the distance, and, in the ideal confidence image, it is characterized by a black color that denotes high confidence inside the object and null outside it.

The proposed MRF algorithm uses the following parameters for the restoration process: 128×128 8-bit per pixel images, 256 gray levels, a first-order neighbourhood system, a variance $\sigma_z^2 = 846$, a logarithmic scheduling for temperature, and an initial temperature 4000. The side of each 128×128 image is fixed equal to 1.4 m and the bottom of the scene, represented by white pixels, is 4.9 m far from the antenna. The confidence threshold was fixed in accordance with the highest side lobe level equal to -13 dB. Then, the threshold $T_C$ was fixed equal to 22% of the average of the 100 highest values of confidence (i.e., $T_C$ = 40). This threshold was also used to select the samples used for the variance computation related to the noise model of the confidence map.

Figures 1(c) and 1(d) show the reconstructed range image and the segmented confidence image, respectively. Figure 1(c) was obtained after a point-by-point AND operation between the restored confidence image and the reconstructed range image at the output of the MRF process (to retain only “confident” points). The result is twofold: first, the algorithm removes holes and side-lobe effects from inside and outside objects, respectively; secondly, the final confidence map is a binary image that separates confident points from non-confident ones. Therefore, the restored confidence map represents a binary segmentation of the scene, where 1 (black) means the presence of an object and 0 (white) represents the scene background. The related edge map is shown in Fig. 1(e). One can notice the good accuracy of the segmentation despite the quality of the initial images. These results represent good approximations of the ideal map and images.

To verify the improvement of the proposed algorithms over other techniques suitable for this type of reconstruction, the mean square error (*MSE*), the relative percentage *MSE* (*RMSE*) between the actual and estimated *Z* data, and segmentation error (to evaluate the correct retrieval of the object shapes) have been considered. Table A provides the results of a comparative analysis performed by applying to the above-considered scene some probabilistic and non-probabilistic methods. Row A reports the results obtained by keeping those pixels of the range image corresponding to the pixels in the confidence image that are above a fixed threshold (AND operation). Also in this case, such a threshold was chosen according to the highest side-lobe level. Although the number of pixels above the threshold is larger than in the ideal case, a lot of holes are present in the reconstructed image increasing the error. Thus, this approach gives the worst result, as it performs only a punctual analysis of the images. Row B reports the results obtained by a technique consisting in the application of an MRF algorithm to the range map obtained after an AND operation with the confidence map manually thresholded to remove residual

holes and restore object shapes. This technique adopts a dual process, one for reconstruction and the other for edge detection (line process [10]) and does not exploit the confidence information. This result is the best obtained using alternative MRF-based methods starting from adequately thresholded maps to decrease as much as possible the initial error. The range image obtained after the above mentioned AND operation (see Row A) has been processed also by using the median filter and the K-nearest neighbourhood average filter. Such techniques are often adopted to reconstruct range images (for more details, see [9]). The results reported in Rows C and D are the best among those obtained by attempting different window dimensions and different values of the K parameter. Row E shows the results of the proposed techniques: it is worth to notice that all the errors are lower than in previous methods. Finally, Row F presents a complementary case that consists in using the ideal confidence map for the reconstruction. It can be noticed a very precise recovery of the 3D information, proving that the better the S estimate, the more precise the reconstructed Z map.

Finally, we consider a real example of a scene composed by 6 cinder blocks placed at slightly different distances, a fixed wrench horizontally placed over the highest blocks, and an adjustable wrench horizontally placed on two vertical blocks. The images were acquired with an acoustic lens sensor [24]. The scene is about 2 m far from the array and the frontal surfaces of the blocks are not parallel to the array plane but slightly inclined [24]. Figures 2(a) and 2(b) show the actual range and confidence images composed of 141×141 pixels covering an area of 1×1 $m^2$. Figures 2(c), 2(d), and 2(e) show the reconstructed range image, the segmented confidence image, and the related edge map, respectively, obtained by the proposed method. Overall, the 3D-scene structure seems well determined also in this case.

## 4. CONCLUSIONS

In this paper, we have presented a probabilistic methodology for the integration of confidence information (directly extracted by an acquisition system) aimed at the reconstruction and segmentation of underwater 3D acoustic images. Range and confidence images have been modelled as random fields affected by Gaussian noise. An MRF-based process is proposed proposing an energy functional whose minimization (in the MAP sense) leads to the joint reconstruction /restoration/segmentation of the images. The functional process is devised incorporating physical constraints allowing a more accurate estimation. Owing to the MRF approach, confidence information is actively used in the reconstruction phase leading to good performances. The final segmentation of the confidence image allows to discriminate between object(s) and background as well as different objects making it possible a easy recovering of the shape for subsequent higher level tasks (e.g., recognition).


## ACKNOWLEDGEMENTS

The authors would like to thank Dr. K.M. Houston (Draper Laboratory, USA), who kindly provided the real data.


## REFERENCES


[1] A.K. Jain, P.J. Flynn, (Eds.), *Three-Dimensional Object Recognition Systems*, Amsterdam: Elsevier, 1993.

[2] R. Szelinsky, *Bayesian Modeling of Uncertainty in Low-Level Vision*, Boston: Kluver Ac. Publ., 1989.

[3] R.O. Nielsen, *Sonar Signal Processing*, Boston: Artech House, 1991.

[4] M. Okino, Y. Higashi, "Measurement of Seabed Topography by Multibeam Sonar Using CFFT", *IEEE Jour. Ocean. Engin.*, Vol. OE-11, pp. 474-479, October 1986.

[5] R.F. Wagner, S.W. Smith, J.M. Sandrik, H. Lopez, "Statistics of Speckle in Ultrasound B-Scans", *IEEE Trans. on Sonics and Ultrasonics*, Vol. 30, pp. 156-163, May 1983.

[6] E. Jakeman, R.J. Tough, "Generalized *K* distribution: a statistical model for weak scattering", *Jour. Opt. Soc. Amer.*, Vol. 4, pp.1764-1772, September 1987.

[7] J.L. Marroquin, *Probabilistic Solution of Inverse Problems*, Ph.D. Thesis, MIT, Boston, 1985.

[8] R.C. Jain, P.J. Besl, "Three-Dimensional Object Recognition", *ACM Computing Survey*, Vol. 17, pp. 75-145, March 1985.

[9] A.K. Jain, R. Hoffman, "Segmentation and Classification of Range Images", *IEEE Trans. on Pattern Analysis and Machine Intelligence*, Vol. 9, pp. 608-620, September 1987.

[10] S. Geman, D. Geman, “Stochastic relaxation, Gibbs distribution, and Bayesian restoration of images”, *IEEE Trans. on Pattern Anal. Machine Intell.*, Vol. PAMI-6, pp. 721-741, November 1984.

[11] A. Blake, A. Zisserman, *Visual Reconstruction*, Cambridge: MIT Press, 1987.

[12] B. Günsel, E. Panayirci, "Segmentation of Range and Intensity Images using Multiscale Markov Random Field Representations", *Int. Conf. on Image Proc.*, Austin (USA), pp. 187-191, October 1994.

[13] A.K. Jain, S.G. Nadabar, "MRF Model-based Segmentation of Range Images", *3rd Int. Conf. on Computer Vision*, Osaka, pp. 667-671, 1994.

[14] B. Günsel, A.K. Jain, "Visual Surface Reconstruction and Boundary Detection using Stochastic Models", *11th Int. Conf. on Pattern Rec.*, The Hague (The Netherlands), pp. 343-346, 1994.

[15] G. Zhang, A. Wallace, "Physical Modeling and Combination of Range and Intensity Edge Data",

*Computer Vision and Image Understanding*, Vol. 58, No. 2, pp. 191-220, September 1993.

[16] L.V. Subramaniam, R. Bahl, "Segmentation and Surface Fitting of Sonar Images for 3D Visualization", *Proc. 8th Int. Symp. on Unmanned Untethered Submersible Technology*, Durham (USA), pp. 290-298, Sept. 1995.

[17] R.S. Beattie, S.C. Elder, "Side Scan Sonar Image Restoration using Simulated Annealing and Iterative Conditional Modes", *Int. Conf. on Sonar Signal Proc.*, Loughborough (UK), pp. 161-167, 1995.

[18] S. Show, J. Arnold, "Automated Error Detection in Multibeam Bathymetry Data", *Proc. IEEE OCEANS '93*, Victoria (Canada), Vol. II, pp. 89-94, 1993.

[19] S. Dugelay, J.M. Augustin, C. Graffigne, "Segmentation of multibeam acoustic imagery in the exploration of the deep sea bottom", *13th Int. Conf. on Pattern Rec.* , Vienna, August 1996, pp. 437-445.

[20] V. Murino, "Acoustic Image Reconstruction by Markov Random Fields", *Electronics Letters*, Vol. 32, N. 7, March 1996, pp. 697-698.

[21] V. Murino, A. Trucco, C.S. Regazzoni, "A Probabilistic Approach to the Coupled Reconstruction and Restoration of Underwater Acoustic Images", *IEEE Trans. on Patt. Anal. and Mach. Intell.*, Vol. 20, No. 1, January 1998.

[22] B. Günsel, A.K. Jain, E. Panayirci, "Reconstruction and Boundary Detection of Range and Intensity Images using Multiscale MRF Representations", *Comp. Vision and Image Understanding.*, Vol. 63, No. 2, March 1996, pp. 353-366.

[23] T.L.Henderson, S.G.Lacker, "Seafloor Profiling by a Wideband Sonar: Simulaton, Frequency-Response, Optimization, and Results of a Brief Sea Test", *IEEE Jour. Ocean. Engin.*, Vol. 14, pp. 94-107, Jan. 1989.

[24] K.M. Houston, "Three-Dimensional Acoustical Imaging Using Micromechanical Hydrophones", *Proc. IEEE OCEANS 95 MTS*, San Diego (CA, USA), pp. 1174-1182, October 1995.

| Row | Method adopted | *MSE* | *RMSE* | Segmentation error |
|---|---|---|---|---|
| A | Simple threshold | 93.1 $cm^2$ | 0.041 % | 591 pixels |
| B | MRF process on Z after AND with S map | 78.0 $cm^2$ | 0.036 % | N.A. |
| C | Median filter | 146.13 $cm^2$ | 0.0635 % | 776 pixels |
| D | K-nearest neighbor filter | 33.72 $cm^2$ | 0.0141 % | 704 pixels |
| E | Proposed algorithm | 18.24 $cm^2$ | 0.0077 % | 359 pixels |
| F | Proposed algorithm using ideal S | 0.15 $cm^2$ | 0.000073 % | 0 pixels |

**Table A**. Comparative results in terms of *MSE*, *RMSE*, and segmentation errors for the proposed techniques and other algorithms suitable for the problem (N.A. = not applicable). See text.

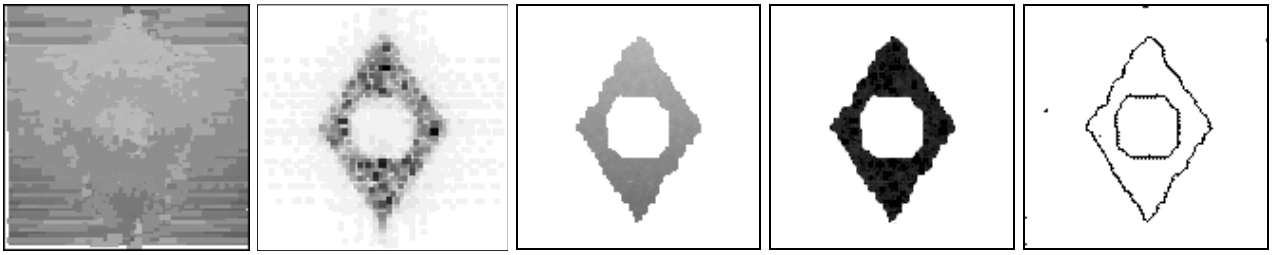

(a) (b) (c) (d) (e)

**Figure 1**. Acoustic images obtained by the beamforming for the simulated example: (a) noisy range image; (b) noisy confidence image; (c) reconstructed range image; (d) segmented confidence image; (e) related edge image.

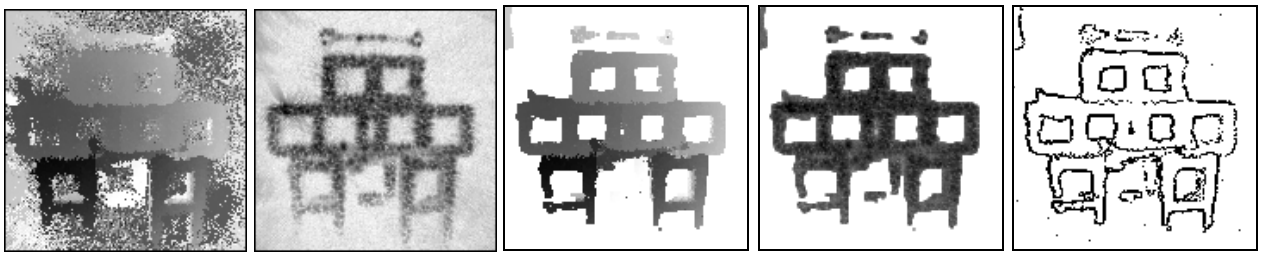

(a) (b) (c) (d) (e)

**Figure 2**. Images obtained by the beamforming and results of the proposed algorithm: (a) noisy range image; (b) noisy confidence image; (c) reconstructed range image; (d) segmented confidence image; (e) related edge image.